10.1098/rspa.2004.1279

THE ROYAL SOCIETY

Analytical approximation of the percolation threshold for overlapping ellipsoids of revolution

By Y.-B. Yi[1] and A. M. Sastry[1,2]

[1]*Department of Mechanical Engineering and*
[2]*Department of Biomedical Engineering, University of Michigan, Ann Arbor, MI 48109-2125, USA* (amsastry@umich.edu)

Received 16 April 2003; revised 12 December 2003; accepted 12 January 2004; published online 11 May 2004

Analytic approximations for percolation points in two-dimensional and three-dimensional particulate arrays have been reported for only a very few, simple particle geometries. Here, an analytical approach is presented to determine the percolative properties (i.e. statistical cluster properties) of permeable ellipsoids of revolution. We generalize a series expansion technique, previously used by other authors to study arrays of spheres and cubes. Our analytic solutions are compared with Monte Carlo simulation results, and show good agreement at low particle aspect ratio. At higher aspect ratios, the analytic approximation becomes even more computationally intensive than direct simulation of a number of realizations. Additional simulation results, and simplified, closed-form bounding expressions for percolation thresholds are also presented. Limitations and applications of the asymptotic expressions are discussed in the context of materials design and design of sensor arrays.

Keywords: percolation; ellipsoid; cluster; analytic; series expansion; sensors

1. Introduction

The importance of percolation phenomena in materials design cannot be overstated. Selection of particle shapes, sizes and volume fractions of phases in heterogeneous or porous materials often begins with a determination of criticalities in interconnections, particularly in their effect upon mechanical, conductive or magnetic properties. We define the key percolation parameter as the fractional volume or mass of a given phase at which it forms a continuous, domain-spanning path across a representative volume element.

It is important to note that for finite areas or volumes, the percolation point is probabilistic, i.e. realizations of the particle arrays generated from the same distributions in particle sizes, shapes, locations and orientations may or may not percolate (e.g. as studied in conductive fibrous arrays, by Sastry *et al.* (1998), Cheng *et al.* (1999), Cheng & Sastry (1999) and Cheng *et al.* (2001) and, previously, in generalized two- and three-dimensional (3D) stick systems, by Balberg & Binenbaum (1983, 1984)). For infinite domains, however, we can define this point precisely as the phase fractional volume at which the mean cluster size of particles of the phase

becomes unbounded. It has been rigorously shown for lattice systems and also for many continuum systems that the (random) percolation point for the finite-volume system converges in probability to the (deterministic) percolation point for an infinite system (Grimmett 1999). Expressions using series expansions of mean cluster sizes to arrive at percolation points for infinite domains render deterministic predictions of percolation point, both in lattice problems (e.g. Sykes & Essam 1964; Coniglio *et al.* 1977*a*, *b*) and continuum percolation problems (e.g. the integral formulation, by Coniglio *et al.* (1977*a*, *b*); the series expansion formulation, by Haan & Zwanzig (1977), Given *et al.* (1990); and the continuum Potts model, by Fortuin & Kasteleyn (1972) and Drory (1996)).

In derivation of analytic solutions for continuum percolation, a series expansion of cluster density is typically used to determine percolation thresholds, via convergence analysis. These series expansions invariably involve an integral expression that arises from the virial theory for a generalized particulate system (e.g. Hill 1955; Balberg 1987; Drory 1996). Such integrals have been evaluated for circles and spheres (Chiew & Stell 1985; Torquato *et al.* 1988), as well as for oriented squares and cubes (Haan & Zwanzig 1977). Also, Quintanilla & Torquato (1996, 1997) reinvestigated the prototypical continuum percolation model, a system of spatially uncorrelated, equally sized circles or spheres, and evaluated its cluster properties using Penrose's (1991) integral expression. Their approximation showed good agreement with those derived by earlier researchers.

It has been widely conjectured, however, that analytical solutions for percolation thresholds can be derived only for a few simple cases of particle geometry (e.g. triangular, simple quadratic and honeycomb lattices (Fisher & Essam 1961; Sykes & Essam 1964) and the one-dimensional continuum model (Drory 1997)). Thus, numerical models have been used to determine percolative properties of arrays of non-circular particles. For example, the now classic work of Kirkpatrick (1973) revealed a power-law relationship between conductivity and bond fraction, useful in determining critical volume fraction. Pike & Seager (1974) presented Monte Carlo simulation results illustrating the effects of hardcore interactions, probabilistic and deterministic bonding parameters, and various forms for the bonding function.

Recently, Yi & Sastry (2002) presented probably the first series expansion solution for the generalized problem of arrays of overlapping ellipses, by extending Penrose's (1991) integral technique to analytically estimate percolation thresholds in arrays of ellipses of uniform shape and size. The dependence of percolation threshold on particle aspect ratio was specifically examined, and the analytical approximations showed good agreement with the Monte Carlo simulations performed by the present authors, as well as those reported previously by Xia & Thorpe (1988). This solution technique offered a ready means of investigating percolation in both moderate aspect ratio particle networks, and fibrous materials, in two dimensions. However, two key tasks arise in application of these results, namely, determination of the limitations of the two-dimensional results for three-dimensional systems, i.e. quantification of the relatively higher percolation points in arrays of elliptical versus ellipsoidal particles. As such, analytical approximations of percolative properties of oriented, three-dimensional, high-aspect-ratio phases are highly desirable. Thus, we now extend our previous technique to the three-dimensional problem of percolation in arrays of ellipsoids of revolution. We also develop techniques for efficient numerical implementation of both the analytical and numerical schemes, including a computationally efficient

algorithm for determination of particle overlap. Finally, we validate the analytical approach using three-dimensional Monte Carlo simulations, and compare both analytical and numerical results with previously reported simulation results.

2. The series expansion for three-dimensional overlapping particles

We define $g(r_i, r_j)$ as the probability that two particles positioned at r_i and r_j are directly connected, by closing the edge $\{r_i, r_j\}$. We also define the function g_1 as the probability that the particle centred at r is connected to the graph G, which is formed by closing the edges $\{r_i, r_j\}$ in $\{r_1, r_2, \ldots, r_k\}$; g_2 is defined as the probability that the graph G is connected. Using these definitions, we write an integral representation for the density of clusters (number of clusters per particle) containing k particles from the conventional theories of statistics, as

$$n_k = \frac{\rho^{k-1}}{k!} \int \mathrm{d}r_1 \int \mathrm{d}r_2 \cdots \int \mathrm{d}r_{k-1} \exp\left\{ -\rho \int g_1(r; r^{\langle k \rangle})\, \mathrm{d}r \right\} g_2(r^{\langle k \rangle}). \tag{2.1}$$

which can be expanded in a Taylor series as

$$n_k = \sum_{i=0}^{\infty} (-1)^i \frac{\rho^{k-1+i}}{k!i!} \int \mathrm{d}r_1 \int \mathrm{d}r_2 \cdots \int \mathrm{d}r_{k-1} \left[\int g_1(r; r^{\langle k \rangle})\, \mathrm{d}r \right]^i g_2(r^{\langle k \rangle}). \tag{2.2}$$

These relations, though originally derived in the context of Poisson points (Penrose 1991) and circular/spherical particles (Quintanilla & Torquato 1996; Torquato 2002), can be written more generally for oriented particles in $\mathbb{R}^3$. We first introduce additional sequential and non-interchangeable degrees of freedom α, β and φ, representing particle rotational angles about the x-, y- and z-axes, respectively. Introduction of these angular degrees of freedom requires that the previous integration be performed over the domain $r(x, y, z, \alpha, \beta, \varphi)$. We can further modify the original integral equations by introducing probability density functions in the integrand representing particle shapes and sizes, as

$$\begin{aligned} n_k = \frac{\rho^{k-1}}{k!} & \int f(l_1^{(1)}, l_2^{(1)}, \ldots)\, \mathrm{d}l_1^{(1)}\, \mathrm{d}l_2^{(1)} \cdots \mathrm{d}r_1 \int f(l_1^{(2)}, l_2^{(2)}, \ldots)\, \mathrm{d}l_1^{(2)}\, \mathrm{d}l_2^{(2)} \cdots \mathrm{d}r_2 \cdots \\ & \times \int f(l_1^{(k-1)}, l_2^{(k-1)}, \ldots) \exp\left\{ -\rho \int f(l_1^{(k)}, l_2^{(k)}, \ldots) g_1(r; r^{\langle k \rangle})\, \mathrm{d}l_1\, \mathrm{d}l_2 \cdots \mathrm{d}r_k \right\} \\ & \times g_2(r^{\langle k \rangle})\, \mathrm{d}l_1^{(k-1)}\, \mathrm{d}l_2^{(k-1)} \cdots \mathrm{d}r_{k-1}, \end{aligned} \tag{2.3}$$

where l_i is the probability density function for the ith characteristic parameter; r_i is the position vector connecting the centrepoints of particle 0 and particle i. The particle 0 is defined as a particle centred at the origin of the frame of reference.

For a general (triaxial) ellipsoid, the lengths and orientations of the three semi-axes, along with the position of the centre, are required to completely describe the particle shape and position in $\mathbb{R}^3$. For an ellipsoid of revolution (as shown in figure 1), however, one of these axes degenerates, and the shape is determined solely by the orientation of the axis of revolution in $\mathbb{R}^3$, and its radius. The orientation of the axis can be described, for example, by the elevation angle $\theta \in (0, \pi)$ from the z-axis and the rotation angle $\varphi \in (0, \pi)$ about the z-axis, in a spherical coordinate system

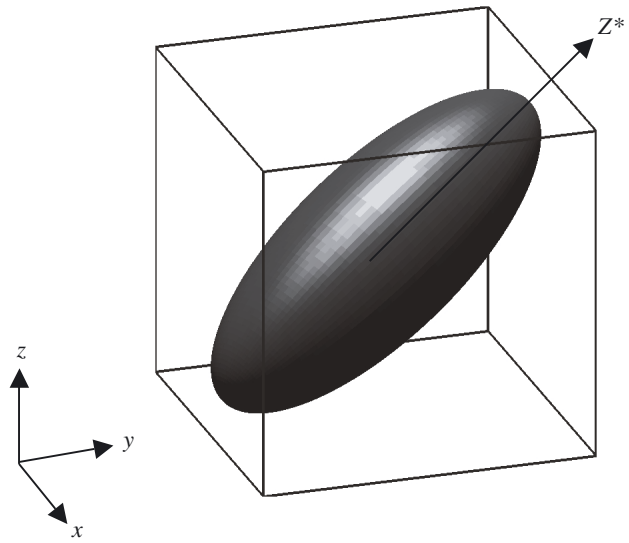

Figure 1. An ellipsoid of revolution. Cell edges mark the extreme values on the ellipsoidal surface in x-, y- and z-directions.

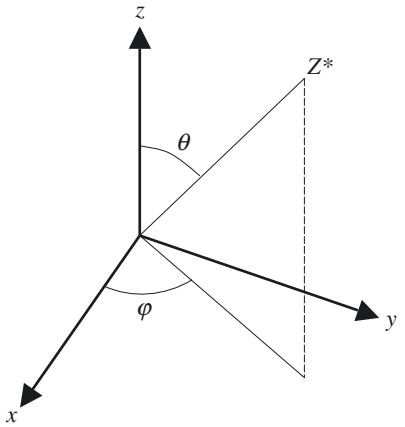

Figure 2. Spherical coordinate system for expression of the orientation of an ellipsoid. Z^* is the axis of revolution for the ellipsoid, and θ and φ are the angular positions of Z^*.

(figure 2). For the problem of uniform ellipsoids of revolution whose geometric centres are positioned by a Poisson process, we have uniform probability density functions for the x, y and z centrepoint coordinates of particles. The density function for angular position φ, also has a uniform density of $1/\pi$ over $(0, \pi)$.

However, the density function for the elevation angle $\theta \in (0, \pi)$ is not uniform. This can be explained as follows. Suppose an event occurs uniformly on a spherical surface of unit radius. The probability that a particle is located in a region of area ΔS is simply $\Delta S/4\pi$, where 4π is the total surface area of the sphere. We can consider a narrow ring $[\theta, \theta+\Delta\theta]$ parallel to the equator, having area $2\pi \sin\theta\Delta\theta$. The probability that the particle is located inside the ring is simply $\sin\theta\Delta\theta/2$. By definition, the probability density function is found by dividing the probability by $\Delta\theta$, resulting

in a non-uniform density of $\sin\theta/2$. This must be considered in simulations, and is discussed later as a possible explanation for discrepancies in reported percolation thresholds.

Using these distributions, can write explicitly, for the cluster density for overlapping ellipsoids of revolution,

$$n_k = \frac{1}{k!}\left(\frac{\rho}{2\pi}\right)^{k-1} \times \int\cdots\left[g_2(r^{\langle k\rangle})\exp\left\{-\frac{\rho}{2\pi}\int g_1(r;r^{\langle k\rangle})\sin\theta\,\mathrm{d}x\,\mathrm{d}y\,\mathrm{d}z\,\mathrm{d}\varphi\,\mathrm{d}\theta\right\} \times\prod_{j=1}^{k-1}\sin\theta_j\right]\mathrm{d}x_2\,\mathrm{d}y_2\,\mathrm{d}z_2\,\mathrm{d}\varphi_2\,\mathrm{d}\theta_2 \cdots\mathrm{d}x_k\,\mathrm{d}y_k\,\mathrm{d}z_k\,\mathrm{d}\varphi_k\,\mathrm{d}\theta_k, \tag{2.4}$$

which can be expanded in a Taylor series as

$$n_k = \sum_{i=0}^{\infty}(-1)^i\frac{1}{k!i!}\left(\frac{\rho}{2\pi}\right)^{k-1+i}\int\cdots\left[\int g_1(r;r^{\langle k\rangle})\sin\theta\,\mathrm{d}x\,\mathrm{d}y\,\mathrm{d}z\,\mathrm{d}\varphi\,\mathrm{d}\theta\right]^i \times\prod_{j=1}^{k-1}\sin\theta_j g_2(r^{\langle k\rangle})\,\mathrm{d}x_2\,\mathrm{d}y_2\,\mathrm{d}z_2\,\mathrm{d}\varphi_2\,\mathrm{d}\theta_2\cdots\mathrm{d}x_k\,\mathrm{d}y_k\,\mathrm{d}z_k\,\mathrm{d}\varphi_k\,\mathrm{d}\theta_k, \tag{2.5}$$

where x_q, y_q, z_q are the x-, y- and z- components of the centrepoint of the qth ellipsoid, and $q = 2,\ldots,k$; ρ is the particle density per unit volume. Note that the integrals in equations (2.4) and (2.5) are evaluated over the domain $r(x,y,z,\varphi,\theta)$, and both g_1 and g_2 are actually either 0 or 1. Again, the $\sin(\theta)$ term in the integrand results from the non-uniform density function of particles along the θ-direction. To generate particles with density function $\sin\theta/2$ for the orientation angle, a set of random numbers $\{\tau\}$ is first generated, with uniform distribution over $[0,1]$. We present here without proof that $\tau^* = \arccos(1-2\tau)$ has density function $\sin\theta/2$, and thus $\{\tau^*\}$ is used to generate particle elevation angles.

The coefficients of the power series of equation (2.4) can be used to obtain the low-density series expansions of mean cluster size, S, and expected cluster size, Q, for a particular particle geometry. These two quantities can be related to cluster density n_k (Quintanilla & Torquato 1996) as

$$S = \sum_{k=1}^{\infty}k^2 n_k, \qquad Q = \frac{1}{\sum_{k=1}^{\infty}n_k}. \tag{2.6}$$

Since cluster density n_k can be expressed in terms of particle density ρ via a power series

$$n_k = \sum_{i=0}^{\infty}c_i\rho^i, \tag{2.7}$$

we rewrite equation (2.6), the series expansion expression of S and Q, in terms of ρ, as

$$S = \sum_{i=0}^{\infty} a_i \rho^i, \qquad Q = \sum_{i=0}^{\infty} b_i \rho^i. \tag{2.8}$$

Percolation thresholds can then be estimated by checking for convergence in S or Q. We point out that Q does not, in fact, diverge at the percolation threshold, since

$$Q = \frac{1}{\sum_{k=1}^{\infty} n_k} < \frac{1}{n_1} = \exp\left\{ \frac{\rho}{2\pi} \int g_1(r; r^{\langle k \rangle}) \sin\theta \, \mathrm{d}x \, \mathrm{d}y \, \mathrm{d}z \, \mathrm{d}\varphi \, \mathrm{d}\theta \right\} \tag{2.9}$$

and, for a finite value of density ρ, the right-hand side of the expression is always bounded. Nevertheless, the low-density series expansion of Q can still be used to provide a reasonable estimate of the percolation threshold, by study of the problem of overlapping spheres (Quintanilla & Torquato 1996).

Among various ways to study series convergence, the use of Padé approximants (Baker & Graves-Morris 1995) offers a reliable technique. In this method, a power series $\Phi(\rho)$ is approximated as a ratio of two series, with the denominator being a series of order l and the nominator being a series of order m, as

$$\Phi(\rho) = \frac{\sum_{i=0}^{m} A_i \rho^i}{\sum_{i=0}^{l} B_i \rho^i + O(\rho^{m+l+1})}. \tag{2.10}$$

The percolation threshold, ρ_c, is reached when Φ diverges. The value of ρ_c (where the subscript 'c' denotes 'critical') can be approximated by one of the real roots of the denominator (Alon *et al.* 1990). To ensure existence of at least one solution, we consider $l \geqslant 1$ approximants, or

$$\Xi(\rho_\mathrm{c}) = \sum_{i=0}^{l \geqslant 1} B_i \rho_\mathrm{c}^i = 0. \tag{2.11}$$

In many applications, including the present work, $l = 1$ is used and ρ_c is determined simply by $\rho_\mathrm{c} = -B_0/B_1$.

3. Contact/overlap criteria

Efficient detection of interparticle contact or overlap is essential for both the analytic approach and Monte Carlo simulations of percolation. For spheres, particle location and geometry are completely defined by particle centrepoint location (x, y, z) and radius a. Two particles are in contact (tangent or overlapping) if $d \leqslant a_1 + a_2$, where d is the distance between the centres; a_1 and a_2 are the radii of the two spheres, respectively. For spheres of uniform size, the overlap criterion can be simply expressed in Cartesian coordinates as

$$\sqrt{(x_1 - x_2)^2 + (y_1 - y_2)^2 + (y_1 - y_2)^2} \rightarrow \begin{cases} \leqslant 2a, & \text{overlap}, \\ > 2a, & \text{separate}. \end{cases} \tag{3.1}$$

For ellipsoids of general orientation, however, it is more difficult to explicitly derive an overlap criterion, due to the added complexity of ellipsoidal surfaces, expressed as

$$\frac{u^2}{a^2} + \frac{v^2}{b^2} + \frac{w^2}{c^2} = 1, \tag{3.2}$$

where

$$\begin{bmatrix} u \\ v \\ w \end{bmatrix} = R \begin{bmatrix} x - x_0 \\ y - y_0 \\ z - z_0 \end{bmatrix}, \tag{3.3}$$

in which x_0, y_0 and z_0 represent the centrepoint position of the ellipsoid, and R is the rotation matrix of the axis of revolution. In $\mathbb{R}^3$, rotations about the x-, y- and z-axes require operations

$$\left.\begin{aligned} R_x(\alpha) &= \begin{bmatrix} 1 & 0 & 0 \\ 0 & \cos\alpha & \sin\alpha \\ 0 & -\sin\alpha & \cos\alpha \end{bmatrix}, \\ R_y(\theta) &= \begin{bmatrix} \cos\theta & 0 & -\sin\theta \\ 0 & 1 & 0 \\ \sin\theta & 0 & \cos\theta \end{bmatrix}, \\ R_z(\varphi) &= \begin{bmatrix} \cos\varphi & \sin\varphi & 0 \\ -\sin\varphi & \cos\varphi & 0 \\ 0 & 0 & 1 \end{bmatrix}. \end{aligned}\right\} \tag{3.4}$$

Because any arbitrary rotation can be decomposed into rotations about each of the three axes, by Euler's rotation theorem, we can write a 3×3 rotation matrix as

$$R = R_x(\alpha)R_y(\beta)R_z(\theta) = \begin{bmatrix} R_{11} & R_{12} & R_{13} \\ R_{21} & R_{22} & R_{23} \\ R_{31} & R_{32} & R_{33} \end{bmatrix}, \tag{3.5}$$

which operates on a vector R. For ellipsoids of revolution about the z-axis, we have $b = c$, and the rotation matrix becomes

$$R = R_y(\theta)R_z(\varphi) = \begin{bmatrix} \cos\theta\cos\varphi & \cos\theta\sin\varphi & -\sin\theta \\ -\sin\varphi & \cos\varphi & 0 \\ \sin\theta\cos\varphi & \sin\theta\sin\varphi & \cos\theta \end{bmatrix}. \tag{3.6}$$

To determine overlap among arbitrarily sized ellipsoids, a commercial equation solver can be used to iteratively solve the pairwise nonlinear equations; interconnectedness is detected by the presence of at least one real solution. Although such a scheme is workable for low-density arrays, it quickly becomes cumbersome for mid-range densities, since the number of connectedness detections grows exponentially with particle number in any given realization.

For the arrays of identical ellipsoids investigated here, however, the efficient overlap detection algorithm of Vieillard-Baron (1972) can be used, described as follows. For two identical ellipsoids of revolution E_1 and E_2, we denote as $\boldsymbol{u}_1$, $\boldsymbol{u}_2$ the unit vectors of the axes of revolution for E_1 and E_2. Each ellipsoid has major axis length $2a$ (along the axis of revolution) and transverse axis length $2b$, and $\boldsymbol{u}$ is the vector connecting the centrepoints of the two ellipsoids. The necessary and sufficient condition for two ellipsoids to have no real point in common, or to be exteriorly tangential, is that the

three following functions (ψ, s_1, s_2), by

$$\xi = \frac{a}{b} - \frac{b}{a}, \tag{3.7}$$

$$t_1 = 4 + \xi^2(\boldsymbol{u}_1 \times \boldsymbol{u}_2)^2 - \frac{|\boldsymbol{u}|}{b^2} + \left(\frac{1}{b^2} - \frac{1}{a^2}\right)\boldsymbol{u}_1 \cdot \boldsymbol{u}, \tag{3.8}$$

$$t_2 = 4 + \xi^2(\boldsymbol{u}_1 \times \boldsymbol{u}_2)^2 - \frac{|\boldsymbol{u}|}{b^2} + \left(\frac{1}{b^2} - \frac{1}{a^2}\right)\boldsymbol{u}_2 \cdot \boldsymbol{u}, \tag{3.9}$$

$$h = t_1 + t_2 - 2 - \frac{\xi^2}{b^2}(\boldsymbol{u}_1 \times \boldsymbol{u}_2) \cdot \boldsymbol{u}, \tag{3.10}$$

$$p = -h, \tag{3.11}$$

$$q = t_1 t_2 - 4, \tag{3.12}$$

$$w = 4h - t_1^2 - t_2^2, \tag{3.13}$$

$$\psi = 4(p^2 - 3q)(q^2 - 3wp) - (9w - pq)^2, \tag{3.14}$$

$$s_1 = h^2 - 2t_1 t_2 - 4, \tag{3.15}$$

$$s_2 = t_1^2 t_2^2 + 8t_1 t_2 - 2h(t_1^2 + t_2^2), \tag{3.16}$$

be positive or zero, and that at least one of the quantities t_1, t_2 and h be negative. We denote function ψ as the *contact function*. Using the relations

$$\left.\begin{aligned} \boldsymbol{u}_1 &= m_1 i + m_2 j + m_3 k, \\ \boldsymbol{u}_2 &= l_1 i + l_2 j + l_3 k, \\ \boldsymbol{u} &= x i + y j + z k, \end{aligned}\right\} \tag{3.17}$$

$$|\boldsymbol{u}| = \sqrt{x^2 + y^2 + z^2}, \tag{3.18}$$

$$\boldsymbol{u}_1 \times \boldsymbol{u}_2 = (m_2 l_3 - m_3 l_2) i + (m_3 l_1 - m_1 l_3) j + (m_1 l_2 - m_2 l_1) k, \tag{3.19}$$

$$(\boldsymbol{u}_1 \times \boldsymbol{u}_2)^2 = (m_2 l_3 - m_3 l_2)^2 + (m_3 l_1 - m_1 l_3)^2 + (m_1 l_2 - m_2 l_1)^2, \tag{3.20}$$

$$(\boldsymbol{u}_1 \times \boldsymbol{u}_2) \cdot \boldsymbol{u} = (m_2 l_3 - m_3 l_2) x + (m_3 l_1 - m_1 l_3) y + (m_1 l_2 - m_2 l_1) z, \tag{3.21}$$

$$\boldsymbol{u}_1 \cdot \boldsymbol{u}_2 = m_1 l_1 + m_2 l_2 + m_3 l_3, \tag{3.22}$$

$$\boldsymbol{u}_1 \cdot \boldsymbol{u} = m_1 x + m_2 y + m_3 z, \tag{3.23}$$

$$\boldsymbol{u}_2 \cdot \boldsymbol{u} = l_1 x + l_2 y + l_3 z, \tag{3.24}$$

we evaluate ψ, s_1, s_2, t_1, t_2 and h.

4. Integral reduction

Because each ellipsoidal particle of revolution has five degrees of freedom, i.e. three Cartesian coordinates to define the particle centre and two angles to define the orientation of the axis of revolution, we have, in the integral expression of cluster density, five integration variables for each dummy particle. These two additional degrees of freedom for ellipsoids, over the three required for spheres or parallel cubes, make computation of the integral expression considerably more intensive; reduction of integral domain is thus of key importance in the analytical approach.

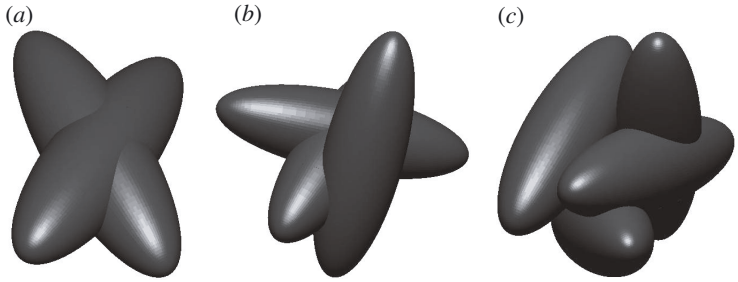

Figure 3. Clusters of (*a*) two, (*b*) three and (*c*) four permeable ellipsoids.

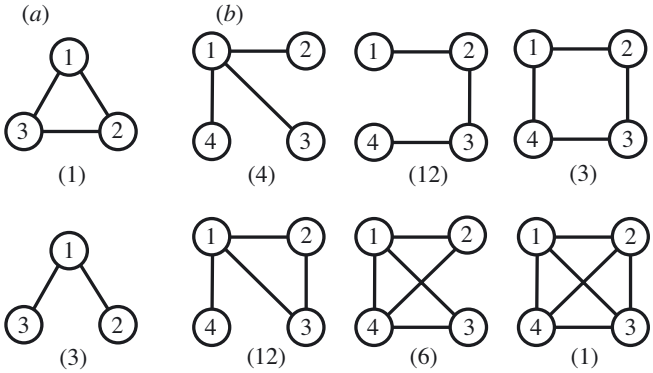

Figure 4. Connected graphs for three-point and four-point integral reductions. Each graph represents a cluster configuration, and each particle in a graph must be connected to at least one of the remaining particles, to form a connected path. The total number of ways to connect particles is the summation of the permutation numbers of all graphs.

(*a*) *Connected graphs*

In the integral expression of cluster density, the integral domain spans $\mathbb{R}^3$, but the integrand is non-zero only when the dummy particles form a connected path. As a result, the actual integral domain comprises a set of finite regions, offering an opportunity to reduce the integration domain. We find by the *arrival method* (Roach 1968) that the number of possible ways to connect k particles is

$$\sum_{k_0<k_1<\cdots<k_i} \frac{(k-1)!}{(k_1-k_0)!\cdots(k_i-k_{i-1})!} 2^{\{(k_0-k_i+(k_1-k_0)^2+\cdots+(k_i-k_{i-1})^2)/2\}} \times (2^{k_1-k_0}-1)^{k_2-k_1}\cdots(2^{k_{i-1}-k_{i-2}}-1)^{k_i-k_{i-1}}, \quad (4.1)$$

where $k_0 = 1$ and $k_i = k$.

There is one and only one way to connect two particles. It can readily be verified that there are four possible ways to connect three particles and 38 ways to connect four particles (Hill 1955), as shown in figures 3 and 4. Because each particle is distinct, we must consider each connection permutation, in addition to the cluster configurations, to calculate the number of possible connection scenarios. The original integral domain is then rewritten as the summation of all the possible connected graphs.

We give an example of our approach for a cluster of three particles, i.e. $k = 3$. We fix the position of particle zero, allowing a double, instead of triple integral expression, as seen by the absence of the term $\mathrm{d}x_1\,\mathrm{d}y_1\,\mathrm{d}z_1\cdots$ from the integral expression of cluster density,

$$n_3 = \frac{1}{6}\left(\frac{\rho}{2\pi}\right)^2 \times \iint \left[g_2(r^{\langle 3\rangle}) \exp\left\{ -\frac{\rho}{2\pi} \int g_1(r; r^{\langle 3\rangle}) \sin\theta \,\mathrm{d}x\,\mathrm{d}y\,\mathrm{d}z\,\mathrm{d}\varphi\,\mathrm{d}\theta \right\} \times \prod_{j=1}^{2} \sin\theta_j \right] \mathrm{d}x_2\,\mathrm{d}y_2\,\mathrm{d}z_2\,\mathrm{d}\varphi_2\,\mathrm{d}\theta_2\,\mathrm{d}x_3\,\mathrm{d}y_3\,\mathrm{d}z_3\,\mathrm{d}\varphi_3\,\mathrm{d}\theta_3. \tag{4.2}$$

We use

$$n_3 = \iint \tag{4.3}$$

as a simplified notation to represent the original integral expression for $k = 3$. Clearly, from the three-point graph (the connected graph consisting of three particles), we have two different cluster configurations with the weight (permutation number) 3 and 1, respectively, as

$$n_3 = 3n_3^* + n_3^{**}, \tag{4.4}$$

where n_3^* represents the probability of the occurrence of the first cluster configuration, in which particle 0 is connected to both particles 1 and 2, but particles 1 and 2 are not connected directly. If B_0 represents a domain such that all particles connected to particle 0 must fall in this domain (but a particle in this domain need not be connected to particle 0), then particles 1 and 2 must be in B_0. Further, if B_1^* represents a domain such that a particle in the domain must be connected to particle 1, then particle 2 must fall outside B_1^*. Thus, particle 1 is in B_0; particle 2 is in B_0 but not in B_1^*. We denote this cluster probability as

$$n_3^* = \int_{B_0} \int_{B_0 \setminus B_1^*} . \tag{4.5}$$

Similarly, n_3^{**} represents the probability of the second cluster configuration in which particles 0, 1 and 2 are all interconnected. If B_1 represents a domain such that all particles connected to particle 1 must fall inside this domain (but a particle inside this domain may not be connected to particle 1), then particle 2 must be inside B_1. Thus, particle 1 is in B_0; particle 2 is in both B_0 and B_1. We thus write

$$n_3^{**} = \int_{B_0} \int_{B_0 \cap B_1} , \tag{4.6}$$

and for the three-particle integration involved in evaluation of n_3 we have

$$n_3 = \iint = 3 \int_{B_0} \int_{B_0 \setminus B_1^*} + \int_{B_0} \int_{B_0 \cap B_1} . \tag{4.7}$$

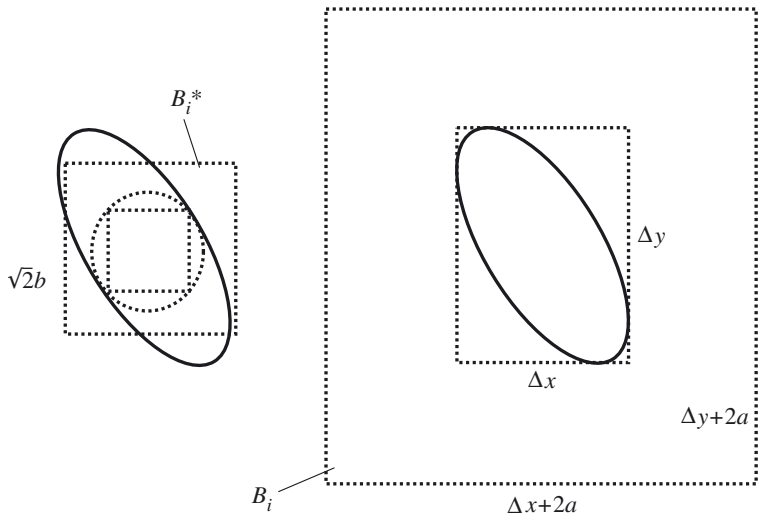

Figure 5. Illustration of B_i and B_i^* for integral reduction. If two particles intersect, the centre of the second particle must be located inside B_i of the first particle; if they do not intersect, the centre must be located outside B_i^*. Note in the 3D case, the cube B_i^* has a length $2/\sqrt{3}b$ instead of $\sqrt{2}b$.

Following the same approach and notation, we have, for the four-particle integration,

$$\begin{aligned} n_4 &= \iiint \\ &= 4\int_{B_0}\int_{B_1\setminus B_0^*}\int_{B_1\setminus(B_0^*\cup B_2^*)} + 12\int_{B_0}\int_{B_1\setminus B_0^*}\int_{B_2\setminus(B_0^*\cup B_1^*)} \\ &\quad + 3\int_{B_0}\int_{B_1\setminus B_0^*}\int_{(B_0\cap B_2)\setminus B_1^*} + 12\int_{B_0}\int_{B_0\cap B_1}\int_{B_0\setminus(B_1^*\cup B_2^*)} \\ &\quad + 6\int_{B_0}\int_{B_0\setminus B_1^*}\int_{B_0\cap B_1\cap B_2} + \int_{B_0}\int_{B_0\cap B_1}\int_{B_0\cap B_1\cap B_2}, \end{aligned} \tag{4.8}$$

where B_i is a cell centred at the origin of the ellipsoid i and has lengths $\Delta x + 2a$, $\Delta y + 2a$ and $\Delta z + 2a$ along the x-, y- and z-axis, respectively; B_i^* represents a smaller cell, centred at the same location, with lengths $4\sqrt{3}/3b = 2.3b$ along all the three axes, as shown in figure 5. We note that $a \geqslant b$ is assumed in the above discussion.

In principle, higher-order integral reduction could be constructed in a similar fashion, but the number of connected paths increases exponentially. In the five-point connected graphs as shown in figure 6, for example, there are 21 possible cluster configurations and 728 possible means of connectivity. An attempt to reduce higher-order integrals would require even more extensive categorization.

It should be pointed out that B_i and B_i^* are actually regions of three-dimensional space in the above integral reduction, and they are brought up to five dimensions by integrating over the whole range of values for the other two dimensions φ and θ. It would be mathematically more elegant to express B_i as a five-dimensional region instead, although it would be less convenient for direct numerical implementation.

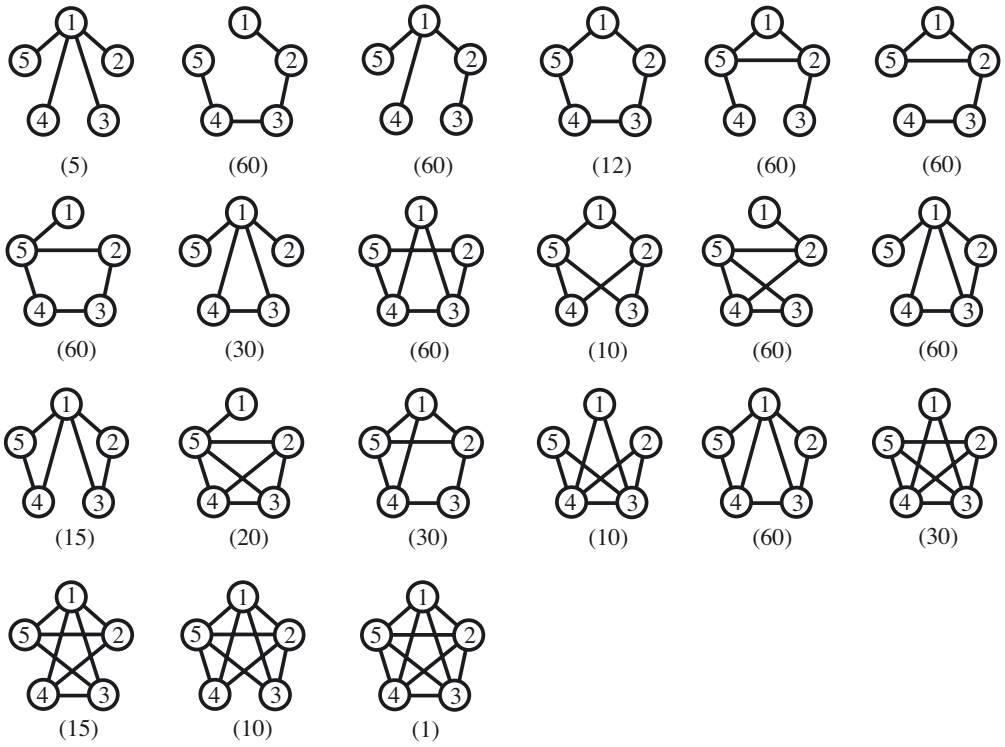

Figure 6. Connected graphs for the five-point integral reduction.

For example, we could write

$$n_3 = 3 \int_{\underline{B}_0} \int_{\underline{B}_0 \setminus \underline{B}_1} + \int_{\underline{B}_0} \int_{\underline{B}_0 \cap \underline{B}_1}, \tag{4.9}$$

where $\underline{B}_i$ represents a five-dimensional region. Note that g_2 in equation (4.2) would be removed in this case, since its value is always unity.

Geometrical symmetry of the first particle at the origin can be considered, in order to reduce computational effort. Here, we reduced the integration domain to the first octant of the 3D space. Indeed, one of the integration variables could be actually eliminated from the integrals if we considered the rotational symmetry of the first particle, although it would not help us much in saving computational effort. The incorporation of this reduction is a non-trivial exercise, which may be part of our future work.

(*b*) *Determination of extreme values of ellipsoids*

To calculate Δx, Δy and Δz in the integral reduction, we define a cell that minimally encompasses each ellipsoid. The smallest, right prismatic cell for each ellipsoid which satisfies this requirement has eight edges tangential to the ellipsoid, marking the maximum and minimum values in the x-, y- and z-directions, respectively (figure 1). To determine the maximum and minimum values of the ellipsoid in the

z-direction, for example, we set

$$\frac{\partial z}{\partial x} = 0, \qquad \frac{\partial z}{\partial y} = 0, \tag{4.10}$$

and, after simplification, obtain

$$\left.\begin{aligned} u &= \pm\sqrt{\frac{a^4(R_{21}R_{32} - R_{22}R_{31})^2}{a^2(R_{21}R_{32} - R_{22}R_{31})^2 + b^2(R_{11}R_{32} - R_{12}R_{31})^2 + c^2(R_{22}R_{11} - R_{12}R_{21})^2}}, \\ v &= -\frac{b^2}{a^2}\frac{R_{11}R_{32} - R_{12}R_{31}}{R_{21}R_{32} - R_{22}R_{31}}u, \\ w &= \frac{c^2}{a^2}\frac{R_{22}R_{11} - R_{12}R_{21}}{R_{21}R_{32} - R_{22}R_{31}}u, \end{aligned}\right\} \tag{4.11}$$

where R_{ij} represents the components of the rotation matrix. For ellipsoids of revolution, the results can be simplified as

$$\begin{bmatrix} u \\ v \\ w \end{bmatrix} = \pm\frac{1}{\sqrt{a^2\cos^2\theta + b^2\sin^2\theta}} \begin{bmatrix} b^2\sin\theta \\ 0 \\ -a^2\cos\theta \end{bmatrix}. \tag{4.12}$$

Hence,

$$\begin{bmatrix} x \\ y \\ z \end{bmatrix} = \pm\frac{1}{\sqrt{a^2\cos^2\theta + b^2\sin^2\theta}} \begin{bmatrix} (a^2 - b^2)\sin\theta\cos\theta\cos\varphi \\ (a^2 - b^2)\sin\theta\cos\theta\sin\varphi \\ a^2\cos^2\theta + b^2\sin^2\theta \end{bmatrix} + \begin{bmatrix} x_0 \\ y_0 \\ z_0 \end{bmatrix}. \tag{4.13}$$

Likewise, setting

$$\frac{\partial y}{\partial x} = 0, \qquad \frac{\partial y}{\partial z} = 0$$

leads to

$$\begin{bmatrix} x \\ y \\ z \end{bmatrix} = \pm\frac{1}{\sqrt{b^2(\cos^2\theta\sin^2\varphi + \cos^2\varphi) + a^2\sin^2\theta\sin^2\varphi}} \times \begin{bmatrix} (a^2 - b^2)\sin^2\theta\sin\varphi\cos\varphi \\ b^2(\cos^2\theta\sin^2\varphi + \cos^2\varphi) + a^2\sin^2\theta\sin^2\varphi \\ (a^2 - b^2)\sin\theta\cos\theta\sin\varphi \end{bmatrix} + \begin{bmatrix} x_0 \\ y_0 \\ z_0 \end{bmatrix}, \tag{4.14}$$

and setting

$$\frac{\partial x}{\partial y} = 0, \qquad \frac{\partial x}{\partial z} = 0$$

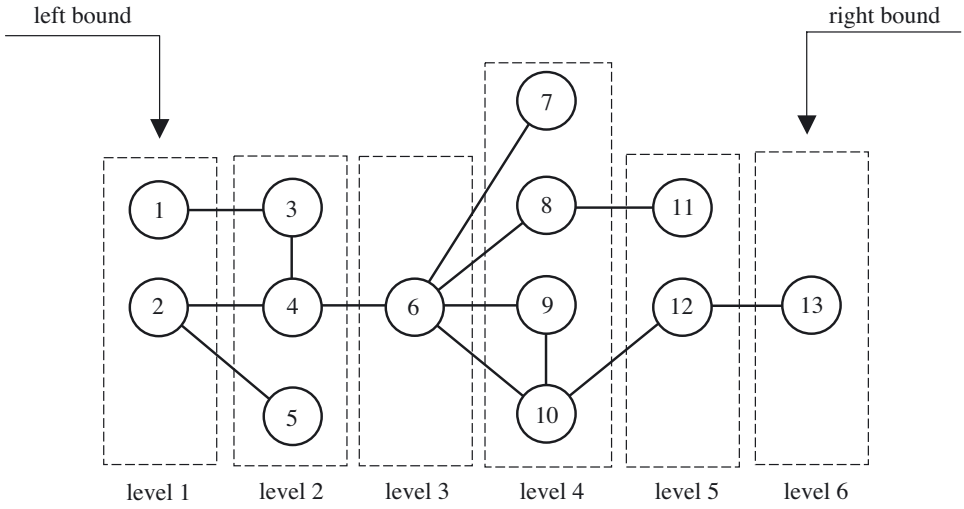

Figure 7. Percolation simulation algorithm for overlapping particles. Cluster architectures show connectivity among members of a cluster.

leads to

$$\begin{bmatrix} x \\ y \\ z \end{bmatrix} = \pm \frac{1}{\sqrt{b^2(\cos^2\theta\cos^2\varphi + \sin^2\varphi) + a^2\sin^2\theta\cos^2\varphi}} \times \begin{bmatrix} b^2(\cos^2\theta\cos^2\varphi + \sin^2\varphi) + a^2\sin^2\theta\cos^2\varphi \\ (a^2 - b^2)\sin^2\theta\sin\varphi\cos\varphi \\ (a^2 - b^2)\sin\theta\cos\theta\cos\varphi \end{bmatrix} + \begin{bmatrix} x_0 \\ y_0 \\ z_0 \end{bmatrix}. \quad (4.15)$$

The cell is thus defined as a block centred at (x_0, y_0, z_0) whose lengths in x, y and z are

$$\Delta x = 2\sqrt{b^2\cos^2\theta\cos^2\varphi + b^2\sin^2\varphi + a^2\sin^2\theta\cos^2\varphi}, \quad (4.16)$$

$$\Delta y = 2\sqrt{b^2\cos^2\theta\sin^2\varphi + b^2\cos^2\varphi + a^2\sin^2\theta\sin^2\varphi}, \quad (4.17)$$

$$\Delta z = 2\sqrt{a^2\cos^2\theta + b^2\sin^2\theta}. \quad (4.18)$$

5. The Monte Carlo simulation algorithm

Researchers have developed a variety of techniques including the 'burning algorithm', or a 'forest-fire model' (Bak & Chen 1989; Dhar 1990; Dhar & Manna 1994) to detect percolation in lattice or continuum networks. We introduce a similar strategy, illustrated schematically in figure 7. Specifically, the particles across one side of the simulation window in a certain direction, say the x-direction, are identified. These particles are the starting points of clusters potentially percolating along the x-direction. We classify these particles as members of level 1. The connectivity between the particles in level 1 and the rest of the particles is then examined. Those

connected are advanced to the second level of cluster architecture. The search procedure continues, generating a cluster architecture in which the members of a certain level can only have connections to the adjacent levels and must have connections to the members at the immediate lower level. Connections to the immediately higher level are checked in each step. The system percolates if at least one particle in the cluster reaches the opposite side of the window in the x-direction. This percolation algorithm is efficient in that we do not check interparticle connectivity inside the same level and we do not check the structure of those clusters isolated from the left boundary.

Results for each condition reported here were generated using 500 separate realizations. The probability of percolation in each network was determined as simply the ratio of the percolating to total number of simulations performed. The overlap criterion was validated by numerically computing the excluded volume of pairs of identical ellipsoids with random centres and orientations. The numerically determined excluded volume was found to be almost identical to the exact solution (previously given analytically by Ogston & Winzor (1975)). Equipped with the verified overlap criterion, we then validated the percolation algorithm using the two-dimensional circle problem, and the three-dimensional sphere problem.

There are several different techniques for estimation of percolation threshold in finite system. The simplest approach is to generate a curve of percolation probability p as a function of volume fraction f and define the percolation threshold as the point of maximum slope on the resulting p–f curve (Safran *et al.* 1985). Since the curve is approximately linear in an extended region, the value at the mid-point of the linear portion is typically used in rougher estimations. An alternative and more accurate approach is to obtain p–f curves from a pair of independent simulations with different cell sizes (or equivalently, different particle sizes); the value of f at which the two curves intersect is a good estimate of the percolation threshold f_c (Stauffer 1979; Saven *et al.* 1991). Nightingale (1975) proposed another strategy in which the critical threshold for several different pairs of cell sizes was used to extrapolate results for infinite systems. Later, Garboczi *et al.* (1995), studying thresholds in fields of overlapping ellipsoids, recorded the number of particles at percolation for each realization, and averaged the results for several realizations.

In the present study, however, an alternative strategy is employed: the percolation probability p is plotted against f in a smooth curve by the method of cubic spline fitting; curves are generated for at least three different ellipsoid sizes. The percolation threshold f_c is then estimated by the value of f at which

$$\min\left\{\sum_{0<i<j<m}(p_i - p_j)^2\right\} \tag{5.1}$$

is reached, where m is the number of curves.

6. Results

(*a*) *Effects of aspect ratio*

As with fields of overlapping ellipses (Yi & Sastry 2002), the density of smaller clusters of ellipsoids is higher at low density. Figure 8 shows typical simulation results

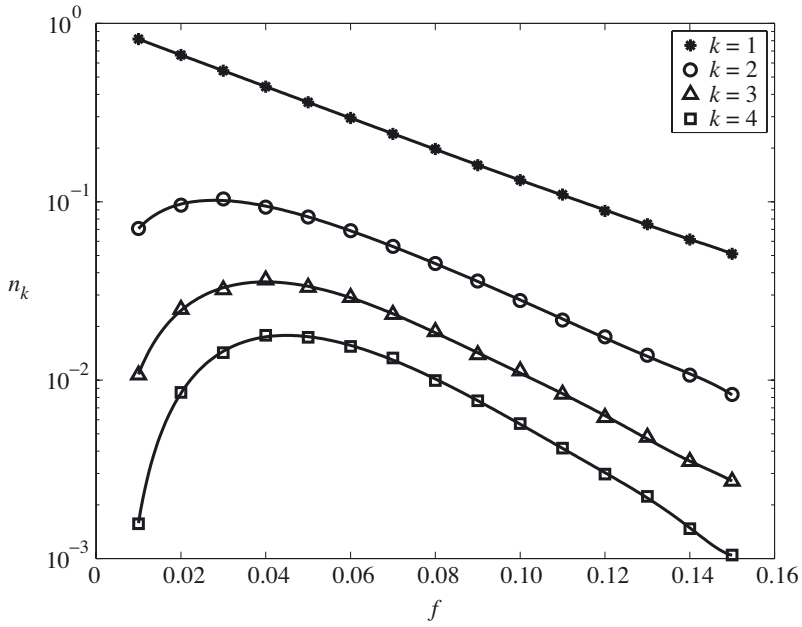

Figure 8. Simulation results for cluster densities in arrays of overlapping ellipsoids. The simulation window is a unit cell; ellipsoids have aspect ratio 10. Averaged results for 500 simulations are shown at each point. Results for cluster sizes $k = 1$, 2, 3 and 4 are shown.

for cluster densities for fields of overlapping ellipsoids of aspect ratio $\varepsilon = 10$. Cluster densities are plotted against volume fraction f. At low particle densities, most particles are isolated, and small clusters dominate. As the volume fraction increases, interparticle connections become more probable, and the density of isolated particles drops, while the number of larger clusters increases rapidly. At high density, most particles are interconnected, and a small number of large clusters arises. In fact, there exists for each cluster size k a certain volume fraction f_k, at which the cluster density of this size is maximum. Specifically, $f_k = 0$ for $k = 1$, and f_k increases monotonically with k.

It has been observed that the n_k–f curve translates to lower volume fractions with increasing aspect ratio. And, since more particles become interconnected at high aspect ratios, percolation threshold is reduced, implying such systems percolate at lower volume fractions. Here, we parametrically studied the effect of aspect ratio on percolation probability, wherein particle aspect ratio was altered, while total particle volume was held constant. Our simulations (figure 9) show that percolation probability p increases monotonically with volume fraction f, and that the p–f curves shift to lower volume fractions, with unchanged slope, for increasing aspect ratio. This implies that particle volume, rather than aspect ratio, predominantly determines the slope of the curve. However, the position of p–f curve along the f-axis is determined primarily by the aspect ratio of the particles.

Thus, in general, the probability of percolation in a finite network is a function of particle volume and aspect ratio, provided that the simulation window size is fixed. For an infinite window size, percolation threshold is deterministic, and expressible as a volume fraction for an aspect ratio only, namely, $f_c(\varepsilon)$. In figure 10 we show

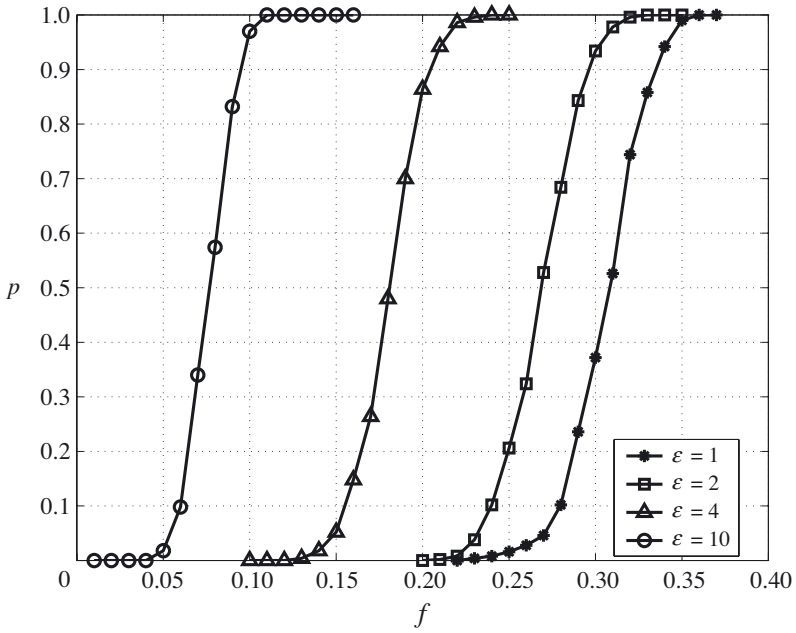

Figure 9. Effect of particle aspect ratio on percolation probability for ellipsoids. Averaged results for 500 simulations, for each of aspect ratios 1, 2, 4 and 10 are shown. Particle sizes are normalized, and volume is normalized by $\frac{4}{3}\pi r^3$, $r = 0.05$.

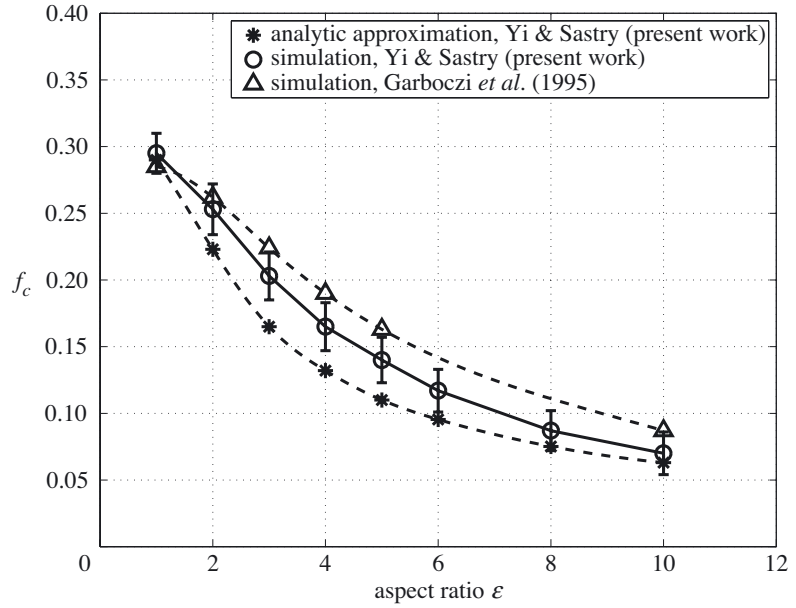

Figure 10. Comparison of analytical approximation and Monte Carlo simulations for the problem of overlapping ellipsoids, compared with simulation results of Garboczi *et al*. (1995). Error bars represent $\pm 1\sigma$ for simulation results, obtained via extrapolation of the linear region of the curves shown in figure 9.

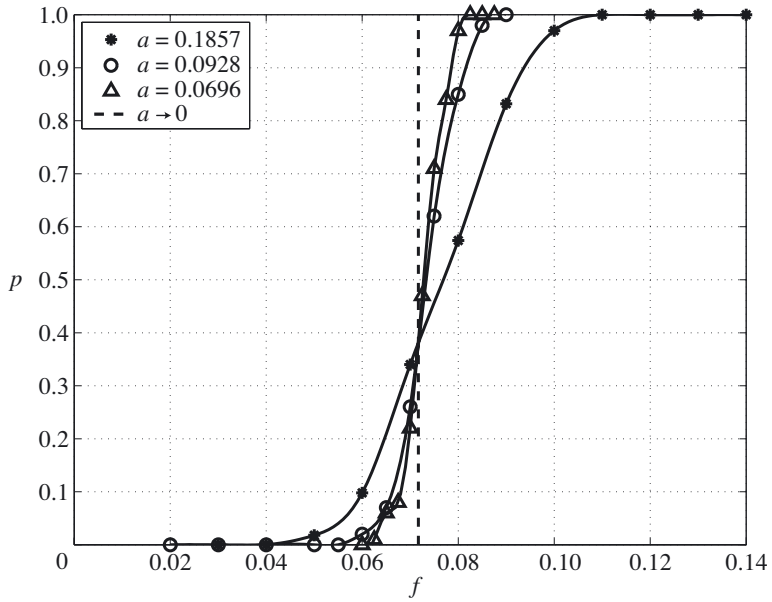

Figure 11. Simulation results for percolation probability versus particle size for arrays of overlapping ellipsoids of aspect ratio 10.

values of percolation thresholds as a function of particle aspect ratio. Both simulation results and analytic approximations are presented, with analytic solutions obtained by application of the series expansion technique discussed in the preceding sections. The four-point connected graphs are used in the integral evaluation for $\varepsilon \leqslant 2$, and the three-point connected graphs are used for $\varepsilon > 2$ due to the numerical demands of the increased complexity in the ellipsoidal particle geometry. The percolation thresholds were estimated by application of the first-order Padé approximants in the power series expansion of the mean cluster number, Q. We see that Q converges much faster than S with large integration intervals; Q was therefore selected for the threshold estimations in this study, though Q leads to an overestimate for spheres. The analytic solution exhibited slight oscillations for different integration intervals; average values for each aspect ratio are presented here.

In determination of percolation threshold from simulations (figure 10), we plot the percolation probability p against f for several particle sizes (figure 11), and then use our least squares scheme to locate the intersecting point of the curves, as discussed previously. The error bars on the simulation curve show the standard deviation in the simulation result, extrapolated from the linear region of the p–f curves. Each curve involved in the approximation was obtained using particles of normalized size $r = \sqrt[3]{ab^2} = 0.03$. Simulation results reported by Garboczi *et al.* (1995) are also shown for comparison.

We note that the simulation results of Garboczi *et al.* lie somewhat above the values obtained here. In order to investigate these differences, we implemented the numerical scheme described by Garboczi *et al.* by successively adding particles to a domain until percolation occurred, and thereupon recording the percolation volume fraction. Our implementation of this technique resulted in a threshold value of 0.0317

for ellipsoids of aspect ratio 20, a number very close to that obtained using our own numerical approach, 0.0315.

We did find, however, that use of either a binary or unbiased distribution function for the particle elevation angle to the z-axis, θ, results in overestimation of the percolation threshold. We found that use of a binary mixture of 0 and $\pi/2$ for the elevation angle θ of the ellipsoids results in an average simulated percolation threshold of 0.046. A uniform distribution in θ yielded an average threshold of 0.035. Garboczi *et al*. (1995) reported a value of 0.0415 for ellipsoids of aspect ratio 20. It is possible that the non-uniformity of the density function of θ (as described earlier in § 2) was overlooked in programming an algorithm for random particle generation by those workers, or that a 'binning' approach was used in specifying elevation angle. Nevertheless, in view of the tolerance range provided by the error bars in figure 10, the two independent sets of simulations are roughly in agreement.

(*b*) *Effect of particle size versus simulation size*

Boundaries in a network simulation impose constraints on the system, and change percolation probability. This scale effect becomes more pronounced as the particle size approaches the window size. Figure 11 shows how simulation window size (or equivalently, particle size) affects the percolation probability in an ellipsoid problem of aspect ratio 10. We investigated the scale effect in simulation by varying the particle size, while maintaining window size and particle aspect ratio.

Each percolation probability curve p–f can roughly be divided into three separate regions: (a) $p \approx 0$; (b) $0 < p < 1$; (c) $p \approx 1$. Accordingly, a given network can be characterized as (a) unpercolated; (b) probabilistic; or (c) percolated. For large particle-to-window sizes, the probabilistic region is relatively wide. In the case of $a = 0.186$, for instance, the p–f curve has a mild slope. The system can percolate at volume fraction as low as 0.05, but an unpercolated realization was also generated at a volume fraction of 0.11. For smaller relative particle sizes, the deterministic regions dominate. In the case of $a = 0.0696$, for instance, the percolation probability becomes non-zero at $f \sim 0.06$, and approaches 100% at $f \sim 0.08$. The 'probabilistic region' is significantly smaller than in the former case. Finally, for the smallest particle-to-window sizes, the 'probabilistic region' disappears entirely, and the percolation status becomes binary. In such a 'percolated' array, a cluster with infinite size exists somewhere in the network, and the probability of percolation is unity; in an 'unpercolated' array, there are no such clusters and the probability of percolation is zero. Therefore, as shown in figure 11, the probability curve becomes nearly vertical as the window size is increased. The curve has a sudden jump at $f_c = 0.072$ when $a = 0$, and the percolation probability curve becomes a step function at the percolation threshold f_c. Thus, the system is unconditionally percolated when $f < 0.072$ and unpercolated when $f \geqslant 0.072$.

The effect of particle size on mean cluster density was also studied, and only a slight correlation was observed. We conclude that boundary conditions generally do not have significant effects on statistical cluster properties in terms of mean values, provided the maximum length of particle is sufficiently smaller than the window size (in general, less than one-fifth or one-tenth). However, boundary conditions typically change standard deviations of statistical properties.

7. Discussion

(a) *Approximation formulae and bounding expressions*

Roach (1968) suggested, and Quintanilla & Torquato (1996) restated, that at low density, n_k can be approximated by

$$n_k \approx \frac{n_1(1-n_1)^{k-1}}{k}. \tag{7.1}$$

This formula is satisfactory at low densities. For spheres of equal size, we expand equation (7.1) in the form of Taylor series as

$$\left.\begin{aligned} n_2 &= 4\eta - 48\eta^2 + 298.7\eta^3 - 1280\eta^4 + O(\eta^5),\\ n_3 &= 21.3\eta^2 - 341.3\eta^3 + 2844\eta^4 + O(\eta^5),\\ n_4 &= 128\eta^3 - 2560\eta^4 + O(\eta^5), \end{aligned}\right\} \tag{7.2}$$

by using the relation $n_1 = \mathrm{e}^{-\rho V_\mathrm{e}} = \mathrm{e}^{-\eta c}$, where ρ is particle density; V_e is excluded volume; η is the reduced density (equal to ρV_0; V_0 is the volume of a single particle); c is V_e/V_0. These results are in excellent agreement with those reported by Quintanilla & Torquato (1996).

It seems, however, neither group extended equation (7.2) to estimate percolation threshold. This is, in fact, possible, since

$$S = \sum_{k=1}^{\infty} k^2 n_k \approx n_1 \sum_{k=1}^{\infty} k(1-n_1)^{k-1}, \tag{7.3}$$

and from a Taylor series expansion, by

$$\frac{1}{(1-x)^2} = \sum_{k=1}^{\infty} k x^{k-1}, \tag{7.4}$$

we have immediately

$$S \approx n_1[1-(1-n_1)]^{-2} = \frac{1}{n_1}. \tag{7.5}$$

This implies an important, intrinsic relation between the mean cluster size and the probability that a particle is isolated. We must note, however, that $1/n_1$ never diverges and therefore this formula is accurate only at low density. The series expansion form of S gives

$$S = \mathrm{e}^{\eta c} = \sum_{k=0}^{\infty} \frac{(\eta c)^k}{k!}, \tag{7.6}$$

whereupon we calculate an estimate of percolation threshold from Padé approximants, i.e. equation (2.10). The form of the approximants can be written succinctly as $[m, l]$. For example, Padé approximant $[2, 1]$ for $f(x)$ is

$$f(x) = \frac{a_2x^2 + a_1x + a_0}{b_1x + b_0} + O(x^4). \tag{7.7}$$

Thus, use of the Padé approximants results in $\eta = 1/c$ for $[0, 1]$; $2/c$ for $[1, 1]$ and $3/c$ for $[2, 1]$, and so forth. The known percolation threshold in volume fraction

is *ca.* 68% for circles, which is bounded by the approximants [3, 1] and [4, 1]; this threshold is *ca.* 29% for spheres, which lies between values evaluated from [1, 1] and [2, 1].

Although this discussion is based on circular and spherical particles, we postulate that similar relations exist for ellipses and ellipsoids, since no limitations were imposed on the particle geometry involved in the original derivation by Roach. Extension of equation (7.7) to particles of a particular shape requires knowledge of their excluded volume. For ellipses, Mack (1954) derived an analytic solution of excluded volume as

$$c = 2 + \frac{8E^2}{\pi^2} \tag{7.8}$$

where E is the elliptic integral

$$E = \frac{1}{\varepsilon}\int_0^{\pi/2} \sqrt{\sin^2\theta + \varepsilon^2\cos^2\theta}\,\mathrm{d}\theta. \tag{7.9}$$

For ellipsoids of revolution, Ogston & Winzor (1975) obtained

$$c = 2 + \tfrac{3}{2}\varepsilon\left\{1 + \frac{1-\zeta^2}{2\zeta}\ln\frac{1+\zeta}{1-\zeta}\right\}\left\{\sqrt{1-\zeta^2} + \frac{\sin^{-1}\zeta}{\zeta}\right\}, \tag{7.10}$$

where

$$\zeta = 1 - \frac{1}{\varepsilon^2}, \qquad \varepsilon = \frac{a}{b}. \tag{7.11}$$

Applying these results, the percolation threshold for ellipses and ellipsoids can be estimated with the aforementioned Padé approximants. Figure 12*a* shows a comparison of the critical area fraction for ellipses between simulations and the approximation formulae. We find that $\eta = 4/c$ is a good estimate for an extensive range of aspect ratios. Figure 12*b* shows a similar comparison for ellipsoids. Simulation results are bounded between $\eta = 2/c$ and $\eta = 3/c$ for $\varepsilon < 10$. For aspect ratios higher than 10, however, the upper and lower bounds change to $\eta = 1/c$ and $\eta = 2/c$, correspondingly.

If $\eta = 4/c$ is used as an estimate of percolation threshold for ellipses as $\varepsilon \to \infty$, then

$$\eta \approx 4\left(2 + \frac{8\varepsilon}{\pi^2}\right)^{-1} \approx \frac{\pi^2}{2\varepsilon} \approx \frac{4.9}{\varepsilon}. \tag{7.12}$$

This is indeed a good approximation, compared with the asymptotic formula $\eta = 4.2/\varepsilon$ obtained by Xia & Thorpe (1988) from direct Monte Carlo simulations.

Likewise, for the ellipsoid problem, it is found that the normalized excluded volume is asymptotic to

$$c = 2 + \tfrac{3}{4}\pi\varepsilon \tag{7.13}$$

when $\varepsilon \to \infty$. If $\eta = 1/c$ is used as an estimate of percolation threshold for ellipsoids of large aspect ratio, then

$$\eta \approx (2 + \tfrac{3}{4}\pi\varepsilon)^{-1} \approx \frac{0.42}{\varepsilon}. \tag{7.14}$$

Garboczi *et al.* (1995) obtained an asymptotic formula $\eta = 0.6/\varepsilon$ for ellipsoids from Monte Carlo simulations. Since significantly lower values were observed in the simulations conducted in this study, $\eta = 0.42/\varepsilon$ may be a more accurate estimate.

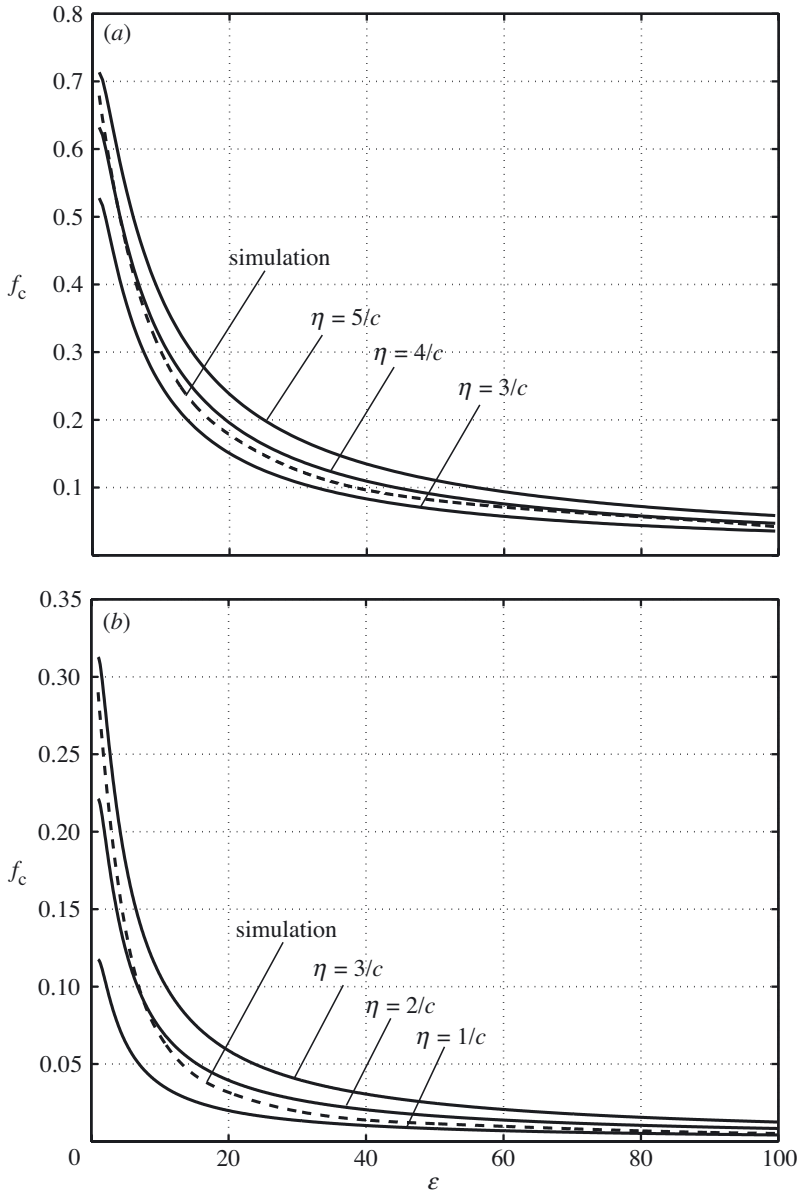

Figure 12. Comparison of simulation results and approximate formulae for (*a*) percolation threshold of ellipses and (*b*) percolation threshold of ellipsoids.

(*b*) *Comparisons between ellipses and ellipsoids*

In table 1 we give the power series expansion forms for cluster density of n_k for ellipsoids of three different aspect ratios, based upon the integral method discussed in the preceding sections. We also present the results for the sphere problem, in order to verify our integration technique for ellipsoids. Please note that the analytic expression for the 'union volume' has not been employed in the integrations for spheres in the

Table 1. *Series expansion form of the cluster density n_k of overlapping ellipsoids for four representative aspect ratios (including spheres)* (η is the reduced density (equal to ρV_0, where ρ is particle density and V_0 is the volume of a single particle).)

	$\varepsilon = 1$			$\varepsilon = 2$			$\varepsilon = 5$			$\varepsilon = 10$		
	n_1	n_2	n_3	n_1	n_2	n_3	n_1	n_2	n_3	n_1	n_2	n_3
η^0	1	0	0	1	0	0	1	0	0	1	0	0
η^1	−7.67	3.835	0	−9.05	4.52	0	−16.2	8.12	0	−60.01	30.01	0
η^2	29.4	−44.83	20.1	40.9	−55.1	16.7	131.8	−166.1	42.7	1801	−3743	2 198
η^3	−75.2	263.9	−313.1	−123.3	340.4	−255.0	−713.0	1841	−1395	−36 026	263 036	−511 004

Table 2. *Previously reported values for percolation points in circular and spherical arrays*

author	circle	sphere
Quintanilla *et al.* (2000)	0.67634	
Rintoul & Torquato (1997)		0.2895
Quintanilla & Torquato (1996)	0.632[a]	0.336[a]
Garboczi *et al.* (1995)		0.285
Lorenz *et al.* (1993)	0.6764	
Rosso (1989)	0.6766	
Xia & Thorpe (1988)	0.68	
Gawlinski & Stanley (1981)	0.676	
Haan & Zwanzig (1977)	0.683[a]	0.295[a]
Fremlin (1976)	0.667	0.286
Pike & Seager (1974)	0.675	0.283
Gayda & Ottavi (1974)		0.283
Ottavi & Gayda (1974)	0.641	
Kurkijarvi (1974)		0.292
Holcomb *et al.* (1972)		0.25
Domb (1972)	0.68	0.29
Roberts (1967)	0.62	

[a]Analytic approximations.

table. As a result, we expect that the computational resolution here is perhaps not as good as that of Quintanilla & Torquato (1996), but acceptable nonetheless. For example, in the series expansion of n_2, the coefficient of η^1 in this work differs by only 4.1% from Quintanilla & Torquato's results, and η^2 differs by 8.5%. These are both within a standard of acceptability of 10%. We note that integration is still required in evaluating n_1, when an analytic expression for g_1 is not applied to equation (2.5). Here, we employed a fivefold integration (with integration variables being the three centre positions, plus two angles of a particle) to evaluate the term related to the integration of g_1, even for spheres. This seemingly redundant work served as a check for the ellipsoidal case, in which no analytic solutions for 'union volume' of multiple particles (three and above) are available. In short, we do not intend to present exact solutions of n_1 for spheres or ellipsoids in table 1. Instead, we present the non-exact but acceptable solutions for the sphere case, in order to validate the integration method used in the ellipsoidal case for $k \geqslant 2$, which is the main focus of the present work.

Table 2 comprises a survey of simulation and closed-form results for percolation points in circular and spherical particle arrays. Table 3 reports previous percolation thresholds in terms of area fraction obtained from simulations and analytical approximations for two-dimensional ellipses. Table 4 reports present and previous results for three-dimensional ellipsoids. The approximate relations are also included in the tables for comparison. Some data in the table were determined via linear interpolation of reported values.

It is unsurprising to find that the critical percolation volume fraction of ellipsoids is lower than that of ellipses, because of the greater likelihood of formation of connected paths in three-dimensional versus two-dimensional networks, assuming the same volume (area) fraction of particle phase. We also find that the percolation threshold of

Table 3. *Previously reported percolation thresholds (in terms of area fraction) from simulations and analytical approximations, for overlapping ellipses*

(Data taken from: A, Xia & Thorpe (1988) simulation; B, Yi & Sastry (2002) simulation; C, Yi & Sastry (2002) series expansion approximation; D, Yi & Sastry (2002) approximation formulae; NA, not available.)

	ε	η	1	5	10	20	50	100	1000
A			0.67	0.46	0.30	0.17	0.080	0.045	0.004 4
B			0.679[a]	0.455	0.301	0.178	0.081 0	0.041 7	0.004 3
C			0.72	0.43	0.31	0.19	0.083	0.040	NA
D		$5/c$	0.714	0.538	0.383	0.238	0.011 1	0.058 4	0.006 13
D		$4/c$	0.632	0.461	0.320	0.196	0.089 6	0.047 0	0.004 91
D		$3/c$	0.052 8	0.371	0.251	0.151	0.068 0	0.035 5	0.003 70

[a]The best currently available numerical estimate is 0.676 339, given by Quintanilla *et al.* (2000).

Table 4. *Present and previous percolation thresholds (in terms of volume fraction) from simulations and analytic approximations for overlapping ellipsoids*

(Data taken from A, Garboczi *et al.* (1995) simulation; B, Yi & Sastry (2002) simulation; C, present work, series expansion approximation; D, present work, approximation formulae.)

	ε	η	1	5	10	20	50	100	1000
A			0.285	0.163	0.087	0.041 5	0.015 0	0.006 95	0.000 60
B			0.290[a]	0.137	0.072 4	0.031 7	0.011 5	0.005 18	0.000 385
C			0.288	0.110	0.063 1	0.025 1	0.010 2	NA	NA
D		$\eta = 3/c$	0.313	0.180	0.108	0.058 7	0.024 7	0.012 5	0.001 27
D		$\eta = 2/c$	0.221	0.124	0.073	0.039 5	0.016 5	0.008 4	0.000 85
D		$\eta = 1/c$	0.118	0.064	0.037	0.020 0	0.008 3	0.004 2	0.000 42

[a]The best currently available numerical estimate is 0.2895, given by Rintoul & Torquato (1997).

ellipsoids drops much more rapidly than that of ellipses as the particle aspect ratio increases. For example, f_c for ellipsoids at $\varepsilon = 10$ is about 0.072. This value is only 25% of that for spheres (0.290). By contrast, f_c for ellipses at $\varepsilon = 10$ is 0.3, which is 44% of the value for circles (0.68). Percolation points for ellipsoidal arrays have stronger dependence on aspect ratio, in that the interparticle connectivity is more sensitive to the particle geometry in the three-dimensional domain than in its two-dimensional counterpart. In fact, considering the limiting case when $\varepsilon \to \infty$ (i.e. zero particle width), it becomes impossible for randomly located three-dimensional particles to overlap, and hence the percolation threshold in terms of particle density is unbounded. However, two-dimensional particles of zero width can still overlap, and the percolation density has an asymptotic and bounded value.

There is a persistent and non-negligible difference between our simulation results and analytical approximations of percolation threshold. The discrepancy has several sources. In simulations, a finite system is used to estimate percolation point for an infinite system, inevitably resulting in an inaccuracy. In the analytic approach, however, percolation threshold is estimated by studying the convergence of an infinite power series, using only the first few terms. Also, the analytic approximation requires a relatively large integration interval due to the present limitation in com-

puter capacity. This results in oscillatory solutions for different integration intervals. We admit that cumulative errors resulting from inaccuracy in successive coefficients in the series expansion, may in fact be non-trivial. The propagation of error from the coefficients of n_k to the percolation threshold estimates must be specifically considered in evaluating the accuracy in the solutions. For example, if the two coefficients used in the Padé approximants have a relative error of 5% each, then the reported percolation threshold could have a relative error of 10%.

Nonetheless, the approximate solution we have presented here will undoubtedly be refined with advances in computing memory and speed. We offer these approaches as a way of eliminating the need for simulations in a wide range of practical materials, through continuing the work of researchers in this area of 'cataloging' percolation points to aid in materials design. Perhaps even more importantly, the combination of analytic and numerical solutions of percolation of penetrable fields allows for direct assessment of sensing probability, since efficient and effective sensor fields must necessarily overlap in order to achieve high probability of sensing events or targets.

Support for this work provided by DARPA and ONR through the Synthetic Multifunctional Materials (SMFM) Program (Dr Leo Christodoulou, Program Manager) is gratefully acknowledged. Support from an NSF PECASE (to A.M.S.), and the W. M. Keck Foundation, is also gratefully acknowledged.

References

Alon, U., Drory, A. & Balberg, I. 1990 Systematic derivation of percolation thresholds in continuum systems. *Phys. Rev.* A **42**, 4634–4638.

Bak, P. & Chen, K. 1989 The physics of fractals. *Physica* D **38**, 5–12.

Baker, G. A. & Graves-Morris, P. 1995 *Padé approximants*, 2nd edn. Cambridge University Press.

Balberg, I. 1987 Recent developments in continuum percolation. *Phil. Mag.* B **56**, 991–1003.

Balberg, I. & Binenbaum, N. 1983 Computer study of the percolation threshold in a two-dimensional anisotropic system of conducting sticks. *Phys. Rev.* B **28**, 3799–3812.

Balberg, I. & Binenbaum, N. 1984 Percolation thresholds in the three-dimensional stick system. *Phys. Rev. Lett.* **52**, 1465–1468.

Cheng, X. & Sastry, A. M. 1999 On transport in stochastic, heterogeneous fibrous domains. *Mech. Mater.* **31**, 765–786.

Cheng, X., Wang, C. W., Sastry, A. M. & Choi, S. B. 1999 Investigation of failure processes in porous battery substrates. Part II. Simulation results and comparisons. *J. Engng Mater. Technol.* **121**, 514–523.

Cheng, X., Sastry, A. M. & Layton, B. E. 2001 Transport in stochastic fibrous networks. *J. Engng Mater. Technol.* **123**, 12–19.

Chiew, Y. C. & Stell, G. 1985 Clustering and percolation in multicomponent systems of randomly centered and permeable spheres. *J. Chem. Phys.* **83**, 761–767.

Coniglio, A., Deangelis, U., Forlani, A. & Lauro, G. 1977*a* Distribution of physical clusters. *J. Phys.* A **10**, 219–228.

Coniglio, A., Deangelis, U. & Forlani, A. 1977*b* Pair connectedness and cluster size. *J. Phys.* A **10**, 1123–1139.

Dhar, D. 1990 Self-organized critical state of sandpile automaton models. *Phys. Rev. Lett.* **64**, 1613–1616.

Dhar, D. & Manna, S. S. 1994 Inverse avalanches in the Abelian sandpile model. *Phys. Rev.* E **49**, 2684–2687.

Domb, C. 1972 Note on series expansion method for clustering problems. *Biometrika* **59**, 209–211.

Drory, A. 1996 Theory of continuum percolation I. General formalism. *Phys. Rev.* E **54**, 5992–6002.

Drory, A. 1997 Exact solution of a one-dimensional continuum percolation model. *Phys. Rev.* E **55**, 3878–3885.

Fisher, M. E. & Essam, J. W. 1961 Some cluster size and percolation problems. *J. Math. Phys.* **2**, 609–619.

Fortuin, C. M. & Kasteleyn, P. W. 1972 Random-cluster model. 1. Introduction and relation to other models. *Physica* **57**, 536–564.

Fremlin, D. H. 1976 Clustering problem—some Monte Carlo results. *J. Phys. Paris* **37**, 813–817.

Garboczi, E. J., Snyder, K. A., Douglas, J. F. & Thorpe, M. F. 1995 Geometrical percolation-threshold of overlapping ellipsoids. *Phys. Rev.* E **52**, 819–828.

Gawlinski, E. T. & Stanley, H. E. 1981 Continuum percolation in 2 dimensions—Monte Carlo tests of scaling and universality for non-interacting disks. *J. Phys.* A **14**, L291–L299.

Gayda, J. P. & Ottavi, H. 1974 Clusters of atoms coupled by long-range interactions. *J. Phys. Paris* **35**, 393–399.

Given, J. A., Kim, I. C., Torquato, S. & Stell, G. 1990 Comparison of analytic and numerical results for the mean cluster density in continuum percolation. *J. Chem. Phys.* **93**, 5128–5139.

Grimmett, G. 1999 *Percolation*, 2nd edn. Springer.

Haan, S. W. & Zwanzig, R. 1977 Series expansions in a continuum percolation problem. *J. Phys.* A **10**, 1547–1555.

Hill, T. L. 1955 Molecular clusters in imperfect gases. *J. Chem. Phys.* **23**, 617–622.

Holcomb, D. F., Iwasawa, M. & Roberts, F. D. K. 1972 Clustering of randomly placed spheres. *Biometrika* **59**, 207–209.

Kirkpatrick, S. 1973 Percolation and conduction. *Rev. Mod. Phys.* **45**, 574–588.

Kurkijarvi, J. 1974 Conductivity in random systems. 2. Finite-size-system percolation. *Phys. Rev.* B **9**, 770–774.

Lorenz, B., Orgzall, I. & Heuer, H. O. 1993 Universality and cluster structures in continuum models of percolation with two different radius distributions. *J. Phys.* A **26**, 4711–4722.

Mack, C. 1954 The expected number of clumps when convex laminae are placed at random and with random orientation on a plane area. *Proc. Camb. Phil. Soc.* **50**, 581–585.

Nightingale, M. P. 1975 Scaling theory and finite systems. *Physica* A **83**, 561–572.

Ogston, A. G. & Winzor, D. J. 1975 Treatment of thermodynamic nonideality in equilibrium studies on associating solutes. *J. Phys. Chem.* **79**, 2496–2500.

Ottavi, H. & Gayda, J. P. 1974 Percolation in a continuous two-dimensional medium. *J. Phys. Paris* **35**, 631–633.

Penrose, M. D. 1991 On a continuum percolation model. *Adv. Appl. Prob.* **23**, 536–556.

Pike, G. E. & Seager, C. H. 1974 Percolation and conductivity: a computer study. *Phys. Rev.* B **10**, 1421–1434.

Quintanilla, J. & Torquato, S. 1996 Clustering properties of d-dimensional overlapping spheres. *Phys. Rev.* E **54**, 5331–5339.

Quintanilla, J. & Torquato, S. 1997 Clustering in a continuum percolation model. *Adv. Appl. Prob.* **29**, 327–336.

Quintanilla, J., Torquato, S. & Ziff, R. M. 2000 Efficient measurement of the percolation threshold for fully penetrable discs. *J. Phys.* A **33**, 399–407.

Rintoul, M. D. & Torquato, S. 1997 Precise determination of the critical threshold and exponents in a three-dimensional dontinuum percolation model. *J. Phys.* A **30**, L585–L592.

Roach, S. A. 1968 *The theory of random clumping*. London: Methuen.

Roberts, F. D. K. 1967 A Monte Carlo solution of a two-dimensional unstructured cluster problem. *Biometrika* **54**, 625–628.

Rosso, M. 1989 Concentration gradient approach to continuum percolation in two dimensions. *J. Phys.* A **22**, L131–L136.

Safran, S. A., Webman, I. & Grest, G. S. 1985 Percolation in interacting colloids. *Phys. Rev.* A **32**, 506–511.

Sastry, A. M., Cheng, X. & Wang, C. W. 1998 Mechanics of stochastic fibrous networks. *J. Thermoplast. Compos. Mater.* **11**, 288–296.

Saven, J. G., Skinner, J. L. & Wright, J. R. 1991 Classical and quantum continuum percolation with hard core interactions. *J. Chem. Phys.* **94**, 6153–6159.

Stauffer, D. 1979 Scaling theory of percolation clusters. *Phys. Rep.* **54**, 1–74.

Sykes, M. F. & Essam, J. W. 1964 Exact critical percolation probabilities for site and bond problems in two dimensions. *J. Math. Phys.* **10**, 1117–1127.

Torquato, S. 2002 *Random heterogeneous materials*, pp. 211–256. Springer.

Torquato, S., Beasley, J. D. & Chiew, Y. C. 1988 Two-point cluster function for continuum percolation. *J. Chem. Phys.* **88**, 6540–6547.

Vieillard-Baron, J. 1972 Phase transitions of the classical hard-ellipse system. *J. Chem. Phys.* **56**, 4729–4744.

Xia, W. & Thorpe, M. F. 1988 Percolation properties of random ellipses. *Phys. Rev.* A **38**, 2650–2656.

Yi, Y. B. & Sastry, A. M. 2002 Analytical approximation of the two-dimensional percolation threshold for fields of overlapping ellipses. *Phys. Rev.* E **66**, 1–8.